Improved representation of diurnal variability of rainfall retrieved from the Tropical Rainfall Measurement Mission Microwave Imager adjusted Precipitation Estimation From Remotely Sensed Information Using Artificial Neural Networks (PERSIANN) system

Yang Hong, Kuo-Lin Hsu, Soroosh Sorooshian, and Xiaogang Gao

Center for Hydrometeorology and Remote Sensing, Department of Civil and Environmental Engineering, University of California, Irvine, California, USA

Received 29 July 2004; revised 30 November 2004; accepted 28 December 2004; published 17 March 2005.

[1] Precipitation Estimation from Remotely Sensed Information Using Artificial Neural Networks (PERSIANN) is a satellite infrared-based algorithm that produces global estimates of rainfall at resolutions of $0.25^\circ \times 0.25^\circ$ and a half-hour. In this study the model parameters of PERSIANN are routinely adjusted using coincident rainfall derived from the Tropical Rainfall Measurement Mission Microwave Imager (TMI). The impact of such an adjustment on capturing the diurnal variability of rainfall is examined for the Boreal summer of 2002. General evaluations of the PERSIANN rainfall estimates with/without TMI adjustment were conducted using U.S. daily gauge rainfall and nationwide radar network (weather surveillance radar) 1988 Doppler data. The diurnal variability of PERSIANN rainfall estimates with TMI adjustment is improved over those without TMI adjustment. In particular, the amounts of afternoon and morning maximums in rainfall diurnal cycles improved by 14.9% and 26%, respectively, and the original 2–3 hours of time lag in the phase of diurnal cycles improved by 1–2 hours. In addition, the rainfall estimate with TMI adjustment has higher correlation (0.75 versus 0.63) and reduced bias (+8% versus −11%) at monthly $0.25^\circ \times 0.25^\circ$ resolution than that without TMI adjustment and consistently shows higher correlation (0.62 versus 0.51) and lower bias (+22% versus −30%) at daily $0.25^\circ \times 0.25^\circ$ scale. This study provides evidence that the TMI, which measures instantaneous rain rates from the TRMM platform flying on a non-Sun-synchronous orbit, enables PERSIANN to capture more realistic diurnal variations of rainfall. This study also reveals the limitation of current satellite rainfall estimation techniques in retrieving the rainfall diurnal features and suggests that further investigation of precipitation generation in different periods of cloud life cycles might help resolve this limitation.

Citation: Hong, Y., K.-L. Hsu, S. Sorooshian, and X. Gao (2005), Improved representation of diurnal variability of rainfall retrieved from the Tropical Rainfall Measurement Mission Microwave Imager adjusted Precipitation Estimation From Remotely Sensed Information Using Artificial Neural Networks (PERSIANN) system, *J. Geophys. Res.*, *110*, D06102, doi:10.1029/2004JD005301.

1. Introduction

[2] Satellite-based precipitation estimation schemes have been developed using microwave (MW)-based, infrared (IR)-based, and combined IR/MW techniques [*Anagnostou et al.*, 1999]. MW observations detect information that is more physically related to precipitation than the longwave (11 μm) IR data, the cloud-top brightness temperature. However, MW instruments currently only reside on low-altitude, polar-orbiting, or other nongeostationary orbiting platforms; thus the low sampling frequency is a major drawback. In contrast, IR data are available almost continuously over time from the geostationary satellites. *Ebert and Manton* [1998] summarized that the MW estimates provided the best instantaneous results and that the IR-based estimates produced the best long-term results. To take advantage of the accuracy of the instantaneous MW estimates and the high temporal resolution of IR estimates, a number of researchers developed techniques that blend the strengths of them to yield combined IR/MW rainfall estimates [*Kummerow and Giglio*, 1995; *Huffman et al.*, 1995; *Xie and Arkin*, 1996; *Xu et al.*, 1999; *Bellerby et al.*, 2000; *Huffman et al.*, 2001; *Miller et al.*, 2001; *Kuligowski*, 2002; *Hong et al.*, 2003; *Kidd et al.*, 2003; *Hong et al.*, 2004; *Joyce et al.*, 2004]. PERSIANN, initially developed as a geostationary IR-based algorithm by *Hsu et al.* [1997], has been operationally producing estimates of rainfall at elemental resolutions of $0.25^\circ \times 0.25^\circ$ and a half-hour after adjustment by using the instantaneous rain rate estimates

0148-0227/05/2004JD005301$09.00

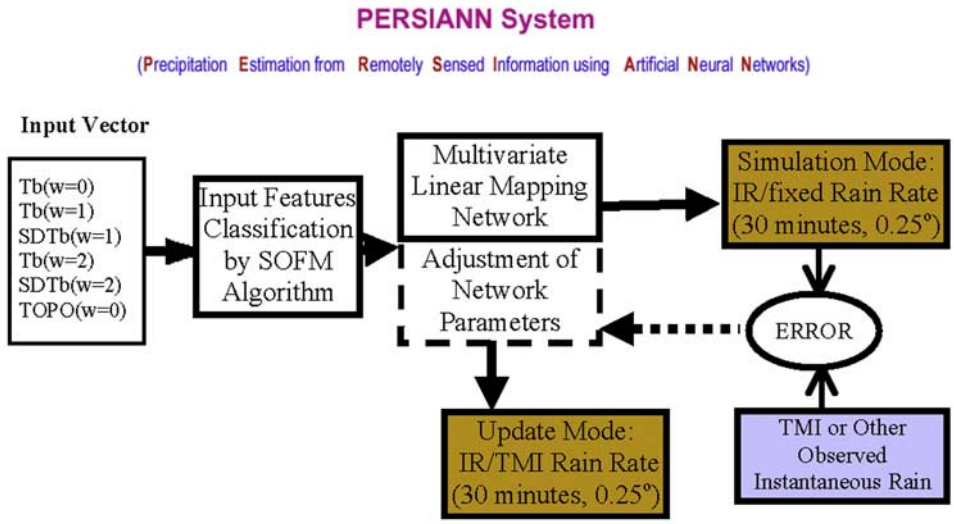

Tb (*w=0*): IR temperature at calculation pixel, window size 0

Tb (*w=1*) mean IR temperature of 3 x 3 pixels, window size 1

SDTb (*w=1*): standard deviation temperature of 3 x 3 pixels

Tb (*w=2*): mean temperature of 5 x 5 pixels, window size 2

SDTb (*w=2*): standard deviation temperature of 5 x 5 pixels

TOPO (*w=0*): surface type (land or water) at calculation pixel

Figure 1. PERSIANN model structure and input-output variables.

from the Tropical Rainfall Measurement Mission (TRMM) Microwave Imager (TMI; *Sorooshian et al.* [2000]). The progress in remote sensing for rainfall estimation has facilitated the investigation of the quality and applicability of these rainfall products. Identifying the diurnal cycle of rainfall from satellite rainfall estimates is an issue with theoretical and practical significance [*Adler et al.*, 1994; *Anagnostou et al.*, 1999; *Sorooshian et al.*, 2002; *Negri et al.*, 2002; *Nesbitt and Zipser*, 2003].

[3] In this paper we compare the rainfall diurnal cycle results from the PERSIANN system with/without the TMI adjustment. Unlike other studies that aim to reveal the features of the rainfall diurnal cycle, the primary goal of this study is to evaluate the quality of rainfall diurnal variability derived from two different stages of PERSIANN outputs: IR-based precipitation estimates from the simulation mode (preadjustment) and the IR/TMI estimates from the update mode (postadjustment). As shown in Figure 1, one of the special features of PERSIANN is that it is designed to run in either the simulation mode or the update mode. Running in the simulation mode, the PERSIANN estimates rainfall based on the high-frequency (48 per day) thermal IR images provided by the geostationary satellites. The update mode enables PERSIANN to combine the high-frequency IR and the low-frequency TMI instantaneous rainfall measurements to estimate rainfall. Hereafter, the simulation mode (preadjustment) and update mode (postadjustment) are referred to as IR/fixed (or based) PERSIANN and IR/TMI PERSIANN, respectively.

[4] The data processing procedure is discussed in section 2, followed by the validation of PERSIANN in section 3. In section 4, the diurnal features of rain intensity derived from IR/TMI and IR/fixed PERSIANN products are compared. Section 5 includes conclusions and discussions of future work.

2. Data and Methodology

2.1. PERSIANN System

[5] The PERSIANN system is a computer-based neural network algorithm that uses the infrared brightness temperature of clouds from geostationary satellites as the basic input variables to retrieve surface rain rates at elemental resolutions of $0.25^\circ \times 0.25^\circ$ and a half-hour. Three specific features have been designed in PERSIANN to improve the estimation. First, the input variables for PERSIANN include a set of IR image features within a moving window of 5×5 pixels surrounding the central target pixel and also the underlying surface type (land or water) (Figure 1). Second, the PERSIANN system classifies the input variables into a number of groups and sets up different submodels (mapping functions) for these groups to correlate the input variables to the output rain rate through a calibration procedure. Third, the PERSIANN includes an adaptive procedure (see Figure 1) that enables the submodels to make self-adjustments according to the feedback from its estimation error (detected from the TMI rain rate) during the operation. For more information, please refer to

Table 1. Data Used in This Study

Data	Coverage and Resolution
Input	
IR images	35°S–35°N, 0.25° × 0.25°, half-hourly
TMI rain rate	35°S–35°N, 0.25° × 0.25°, instantaneous[a]
Output	
IR/fixed rain rate	35°S–35°N, 0.25° × 0.25°, half-hourly
IR/TMI rain rate	35°S–35°N, 0.25° × 0.25°, half-hourly
Validation	
WSR-88D	20°N–50°N and 120°W–65°W, 0.25° × 0.25°, hourly
U.S. rain gauge	20°N–50°N and 140°W–60°W, 0.25° × 0.25°, daily

[a]The non-Sun-synchronous TMI data come in at nonperiodic schedule.

the earlier publications of *Hsu et al.* [1997], *Sorooshian et al.* [2000], and *Hsu et al.* [2002].

2.2. Data Processing

[6] The data used and produced in this study are listed in Table 1. Notably, all of the data are processed at the PERSIANN elemental resolution (0.25° × 0.25°). The IR data are obtained from the NOAA Climate Prediction Center (CPC), which provides global half-hour IR data with a parallax correction for geometric misnavigation of high cloud, corrections of large zenith angles, midpoint interpolation of overlapping satellite coverage, and re-mapping of spatial scales [*Janowiak et al.*, 2001]. The TMI is a nine-channel passive microwave radiometer that operates at five frequencies similar to the frequencies of the Special Sensor Microwave/Imager (SSM/I) instrument. Rainfall estimates from SSM/I onboard Sun-synchronous polar-orbiting satellites are subject to bias in regions where the diurnal cycle of rainfall is pronounced [*Bellerby et al.*, 2000]. However, the TRMM platform for precipitation monitoring flies in a non-Sun-synchronous orbit, which changes the local overpass time and can provide sampling for a complete diurnal cycle over periods of a month or longer; therefore the diurnal estimation is probably better than that from SSM/I over some extended areas [*Kummerow et al.*, 1998]. In addition, TMI is designed with improved instrument quality and higher spatial resolution so that the TRMM microwave rainfall data are considered superior to the SSM/I estimates and used to improve the quality of the IR/fixed estimates.

[7] The initial parameter values of PERSIANN are trained using 1-year (1998) coincident IR and radar rainfall data over the Florida region, where the radar rainfall has good coverage and quality [*Maddox et al.*, 2002]. Afterward, the PERSIANN system can operate in two different modes: simulation (IR/fixed) and update (IR/TMI) mode. In the simulation mode the parameters of PERSIANN are fixed. In the update mode the PERSIANN parameters are sequentially adjusted with a small step size ($\eta = 0.05$) according to the feedback of estimation error detected from the coregistered TMI rain rates (see equation (A5) for details). They are temporally adjusted whenever TMI rain rates are available.

[8] Therefore two sets of rainfall products in year 2002 are generated through the IR/fixed and IR/TMI techniques, respectively (Figure 1). The two modes (IR/fixed versus IR/TMI) have the same initial configurations and the same input of localized IR data in year 2002. The major difference between the two products is that one is adjusted by coregistered TMI observations while the other is not.

[9] To reduce the processing time, the estimation domain (50°S–50°N) of PERSIANN is divided into 96 equally sized rectangular areas (15° × 70° latitude-longitude with overlap on edges to assure smooth transitions between adjacent regions) for parallel computation. For each of the subregions, the self-organizing feature mapping clustering algorithm in PERSIANN system establishes 255 sets of input-output mapping coefficients [*Sorooshian et al.*, 2002]. As a result, 24480 (96 × 255) sets of coefficients, instead of a single set, were used to generate global rainfall estimates. The information (including diurnal features) extracted from input data is implicitly carried by different sets of the input-output mapping coefficients. For example, the afternoon convective clouds and morning stratiform clouds over land would be classified into different sets of input-output mapping coefficients because of their distinctive features. Furthermore, each set of the coefficients makes its own self-adjustment according to the feedback from its estimation error (detected from the TMI rain rate) during the adaptive process (see Figure 1). Not all of the sets of coefficients are observed at every time of day, so certain sets might only be calibrated or adjusted at certain times of day. Therefore the clustering and adaptive procedure enable the PERSIANN system to differentiate and retrieve the diurnal information embedded in geostationary IR cloud imagery and non-Sun-synchronous TMI observations.

[10] The current study area is restricted in the TMI coverage domain of 35°S–35°N, and the validation area is limited to the U.S. continent, where the National Weather Service (NWS) Weather Surveillance Radar-1988 Doppler (WSR-88D) radar and rain gauge data are available.

2.3. Computation of Rainfall Diurnal Cycle

[11] The elemental rain rates (a half-hour and 0.25° × 0.25°) from PERSIANN are first transferred from UTC to the local solar time (LST) according to the geographical location of each grid box. The rainfall diurnal cycle is defined as the monthly mean ($\bar{r}_j$) of half-hour rainfall for each 1° × 1° grid box in the study area.

$$\bar{r}_j = \frac{1}{mp}\sum_{i=1}^{m}\sum_{k=1}^{p} r_{i,j,k}\left(mm.h^{-1}\right)$$

where $r_{i,j,k}$ = rain rate at the elemental PERSIANN pixel (a half-hour and 0.25° × 0.25°), i is day of the month m; j is

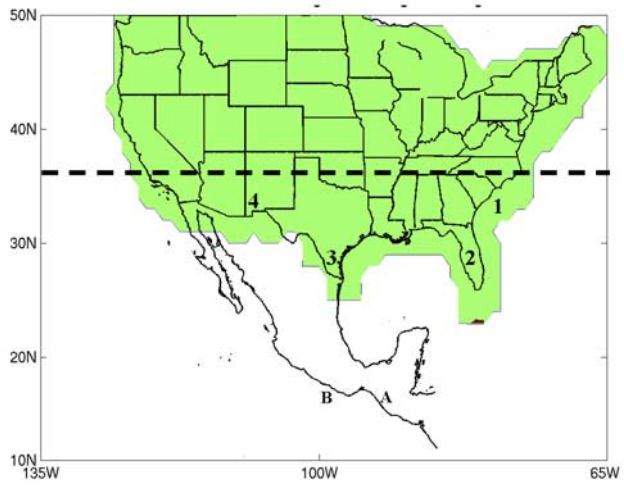

Figure 2. The WSR-88D radar coverage (shading area) and TRMM coverage (under dashed line). Note that the four numbered (1–4) and lettered (A–B) grids from different climatic regions are used for algorithm validation and comparison of rainfall diurnal variability.

time index of half-hour rainfall; and k is location index of elemental pixel in the $1° \times 1°$ grid box (p = 16). In the ideal case without missing data, a $1° \times 1°$ grid box in 1-hour interval for a month of 30 days has 960 ($16 \times 2 \times 30$) elemental rainfall samples to calculate the monthly average. For the purpose of quality control, only a grid box with more than 80% of the maximum possible rainfall samples is used in the study; otherwise a flag of "missing data" is applied to the grid box.

3. Limited Validation

[12] The PERSIANN rainfall estimates are validated using rain gauge and radar data in sections 3.1 and 3.2, respectively. The validation period covers the summer of 2002 (June, July, and August) and the spatial domain (shade region) is shown in Figure 2. Note that grids with zero rainfall also are included for the daily and monthly comparisons. Definitions for the statistical indices, correlation (CORR), root-mean square error (RMSE), bias, skill score, probability of detection (POD), and false alarm ratio (FAR) are adapted from the report of the third Algorithm Intercomparison Project of the Global Precipitation Climatology Project (GPCP; *Ebert* [1996]).

3.1. Daily Rainfall

[13] The rain gauge data used in the validation are the Climate Prediction Center (CPC) real-time daily gauge analysis (see www.cpc.ncep.noaa.gov/research_papers/ncep_cpc_atlas/7/index.html), which is composed of over 7000 stations. These data have already undergone limited automated quality control (duplicate station check, buddy check, and standard deviation check against climatology) and have been processed, using objective analysis interpolation, into 0.25° grid mesh covering the continental United States and Mexico. For this study, some additional quality control was conducted by applying a land/water mask to eliminate regions of missing gauge data in offshore grid boxes. In addition, only those days with more than 400 effective grid data were used in the comparison (about 5% of the data eliminated). Note that the validation domain also is limited within the TMI coverage.

[14] Time series of statistical comparisons of the PERSIANN estimates are illustrated in Figure 3 and Table 2. The IR/TMI estimates outperform IR/fixed estimates in terms of correlation, skill score, POD, and FAR in general, but show higher root-mean square error and bias in a few time periods. The positive bias of the IR/TMI estimates (0.51) referring to the rain gauge data is largely due to the bias of the TMI retrieval technique [*Negri et al.*, 2002]. *Kummerow et al.* [2001] reported a positive bias of 19% over all of the land in the tropical region for the retrieval technique applied to TMI data. The number becomes slightly higher (22%) in this study, after the PERSIANN parameters adjustment using the TMI data. In contrast, the IR/fixed data underestimate rain gauge rainfall by 30%. However, the variability of the skill score shown in Figure 3 suggests that the sequential training approach might suffer from the deficiency of the TMI samples. One way to cope with this may be to enlarge the space domain of training samples.

3.2. Monthly Rainfall

[15] The stage III hourly radar composites, obtained from the National Weather Service's network of operation WSR-88D by the National Centers for Environmental Prediction (NCEP), provide hourly digital precipitation (HDP) radar rainfall estimates at approximately 4×4 km^2 covering the continental United States and its coastal regions [*Maddox et al.*, 2002]. This high spatial and temporal resolution rainfall product provides data useful for verification of satellite rainfall algorithms.

[16] The rainfall estimates derived from IR/TMI and IR/fixed PERSIANN are compared to radar rainfall. Figure 4 (top two panels) shows the scatterplots of seasonally (summer 2002) averaged hourly rain rates (at every local solar hour) over four selected grids (shown in Figure 2). The validation statistics of IR/TMI estimates outperform the IR/fixed data with higher correlation (0.97 versus 0.94), skill score (0.84 versus 0.76), and lower error (0.07 versus 0.11).

[17] Figure 4 (bottom two panels) shows the scatterplots of monthly (July 2002) rainfall over a region of 30°N–36°N and 115°W–105°W. The IR/fixed estimates underestimate heavy rainfall but show lower standard deviation (27 versus 44) and lower root-mean square error (31 versus 37 mm month^{-1}) than the IR/TMI estimates. However, the latter demonstrates better rainfall ratio (1.08 versus 0.89) and higher correlation (0.75 versus 0.63). It is worth mentioning that at the monthly scale the IR/TMI rainfall estimation is not necessarily better than IR/fixed values in terms of root-mean square error, but the routine adjustment of instantaneous TMI rainfall into PERSIANN estimation substantially improves the correlation by 12%, particularly in regions of high rain intensity. The scatterplots given in Figure 4 also show that the IR/fixed estimation has a tendency to systematically underestimate heavy rainfall.

4. Diurnal Cycle of Rainfall

[18] Monthly mean hourly rainfall was computed at the $0.25° \times 0.25°$ resolution and aggregated into a $1° \times 1°$ grid

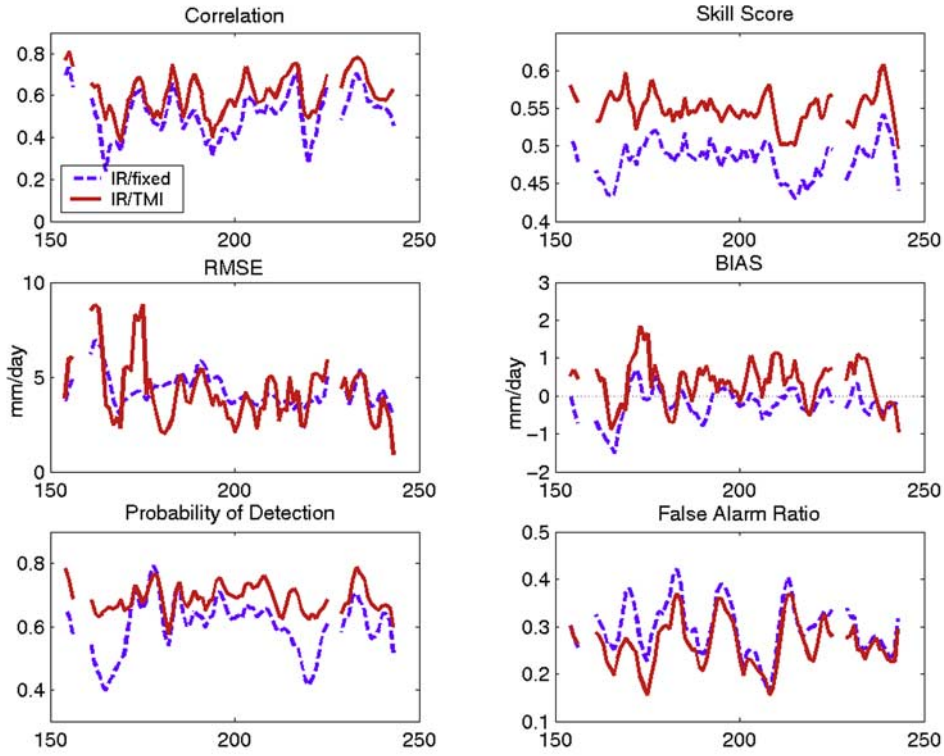

Figure 3. Validation of PERSIANN estimates with U.S. daily rain gauge data at 0.25° × 0.25° resolution over the continental United States (within TRMM coverage) during June, July, and August 2002.

for depicting the rainfall diurnal cycle. Section 4.1 compares the diurnal variations derived from the IR/TMI and the IR/fixed data, and section 4.2 briefly describes the diurnal variability of tropical rainfall from the IR/TMI estimates.

4.1. Comparison of Rainfall Diurnal Variability

[19] Because of the lack of ground rainfall observation with high sampling over the global tropic region, the diurnal variability from the IR/TMI and IR/fixed estimates was compared to WSR-88D data over the continental United States. Note that the radar rainfall also suffers from varying errors (view angle, atmospheric attenuation, the parameterization of Z-R function, and so forth). Additionally, radar does not give direct measurement of precipitation reaching the surface, which might introduce uncertainty in estimates of the diurnal cycle of rainfall.

4.1.1. Diurnal Variability Over Land and Coastal Regions

[20] The following analysis of diurnal variation is based on a 1° grid aggregated from 0.25° elemental grids. To take into account the availability of radar data, the coastal area is therefore determined as the 1° grids mixed with land and sea 0.25° subgrids within the area of WSR-88D radar coverage (see Figure 2).

[21] Figures 5a–5b show the diurnal variation of rain rates over land and coastal areas within the region of 20°N–36°N and 130°W–65°W. The phases of PERSIANN diurnal cycles consistently lag behind the radar cycle. Over land, the IR/TMI diurnal cycle shows a 1-hour lag of the maximum peak, while the IR/fixed diurnal cycle lags behind 2 hours, missing the heavy rainfall occurring in the early stages of convection. *Negri et al.* [2002] also reported a 3-hour lag in the GOES precipitation index (GPI) diurnal cycle. They explained that the IR-based technique determines the highest rain rates from the coldest IR cloud-top brightness temperatures; however, the actual peak rain might already fall before the convective cloud reaches its maximum height.

[22] As shown in Table 3 and Figure 5, the IR/TMI technique captures the phase and amplitude of the radar diurnal cycle better than the IR/fixed approach over both the land and coastal areas. Note that the amplitude is defined as the ratio of the peak rain rate to the mean of diurnal rainfall. In particular, the amplitudes of the diurnal cycle derived

Table 2. Validation Statistics of PERSIANN Estimates With U.S. Daily Rain Gauge Data[a]

	Correlation	Skill	RMSE, mm day^{-1}	Bias, mm day^{-1}	POD	FAR
IR/TMI	0.62	0.64	5.82	0.51	0.69	0.27
IR/fixed	0.51	0.56	5.86	−0.69	0.57	0.34

[a]Averaged from Figure 3. Note that the mean daily rainfall from IR/TMI data is 2.29 mm day^{-1}.

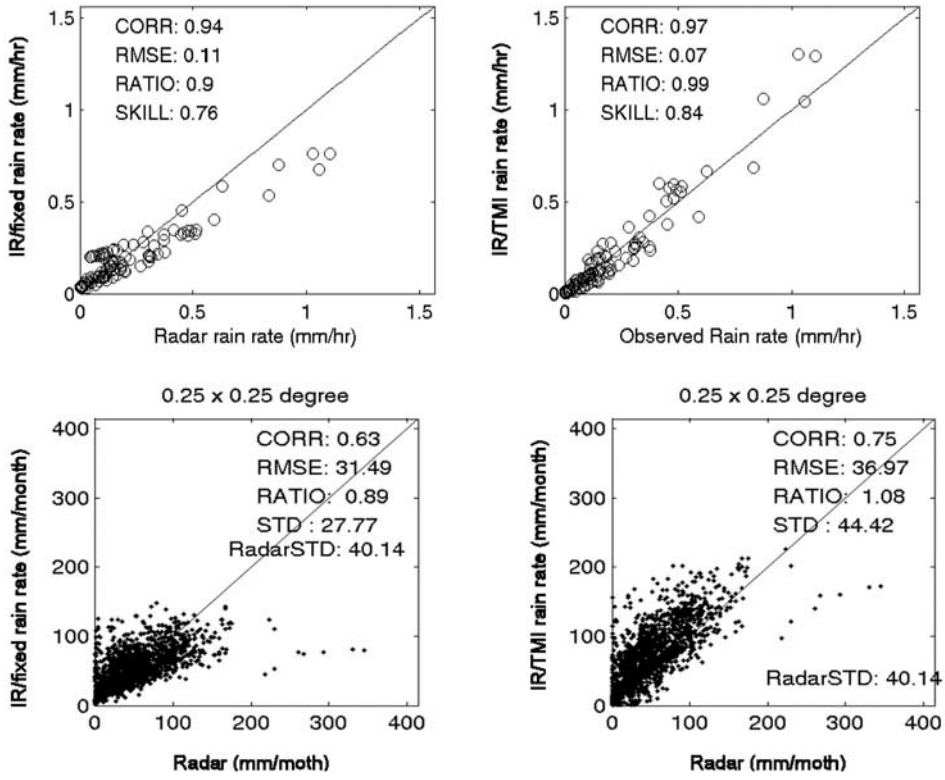

Figure 4. The top two panels show scatterplots of monthly averaged hourly rain rates (at local solar hour) derived from IR/TMI and IR/fixed PERSIANN compared to WSR-88D rainfall over the summer season at the four selected locations (Figure 2). The bottom two panels show scatterplots of monthly (July 2002) rainfall derived from IR/TMI, IR/fixed PERSIANN system, and WSR-88D rainfall at region 30°N–36°N and 115°W–105°W.

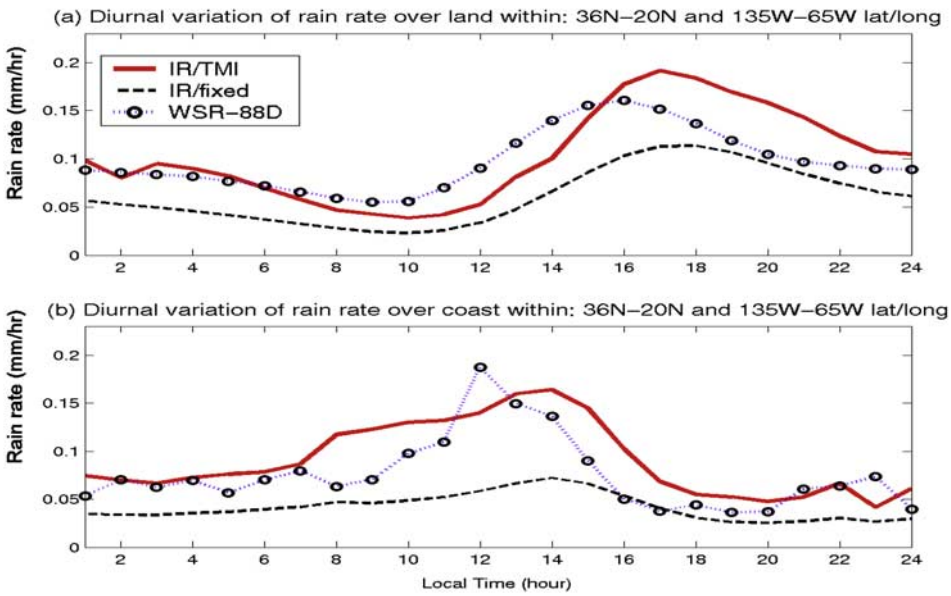

Figure 5. Diurnal variation of rainfall intensity from different data sets over (a) land and (b) over coastal areas. Note that the diurnal variation is averaged at $1^\circ \times 1^\circ$ grids and the coastal areas is defined as the transitional grids between land and ocean where WSR-88D radar data are also available.

Table 3. Statistics of Diurnal Variation of Rain Rates From Two Data Sets Over the Land and the Coastal Areas[a]

	Land (150 Grids of 1° × 1°)					Coastal Areas (15 Grids of 1° × 1°)				
	Correlation	Mean, mm	Maximum, hr^{-1}	SD	Amplitude	Correlation	Mean, mm	Maximum, hr^{-1}	SD	Amplitude
Radar	N/A	0.097	0.165	0.037	1.701	N/A	0.082	0.181	0.037	2.207
IR/fixed	0.817	0.078	0.113	0.028	1.449	0.715	0.054	0.072	0.013	1.333
IR/TMI	0.874	0.108	0.184	0.041	1.703	0.786	0.086	0.164	0.038	1.907

[a]Note that the amplitude is defined as the ratio of peak to mean in the rainfall diurnal cycle. SD, standard deviation; N/A, not applicable.

from radar and IR/TMI rainfall are closer over land (1.701 versus 1.703) and slightly different over the coastal area (2.207 versus 1.907), while the amplitude of the IR/fixed cycle is considerably smaller over the land (1.449) and over the coastal area (1.333). The IR/TMI rainfall data improve, compared to the IR/fixed estimates, the depiction of the amplitude of rainfall diurnal cycle by 14.9% over land and 26% over coastal areas. The IR/TMI also has the standard deviation (SD) of diurnal rain rates closer to the radar data.

[23] Table 3 shows that the IR/TMI overestimates the mean of rainfall diurnal variation by 11% (5%) over land (coastal areas), while IR/fixed data underestimate by 19% (34%) over land (coastal areas). This restates that the TMI adjustment could correct the underestimation of IR/fixed estimates but also introduces positive bias. Note that the results over coastal regions should be viewed with caution because of the small number of grids.

4.1.2. Diurnal Variability of Rainfall Over Four Selected Grids

[24] Figures 6a–6d show the diurnal cycle of seasonally (JJA) averaged rainfall for four 1° × 1° grids in different climate regions (see Figure 2 for the locations). Note the distinct differences in the diurnal rainfall variations among these grids. Grid 1 is located over the Atlantic Ocean and exhibits a pattern of diurnal cycle over the ocean (Figure 6a). Grids 2–4 (Figures 6b–6d) belong to a land pattern, characterized by larger amplitudes during the afternoon through midnight but narrower duration of high rainfall. Grid 2, located over Florida, exhibits the highest peak of diurnal rain intensities (1.3 mm hr^{-1}), while grid 4, located

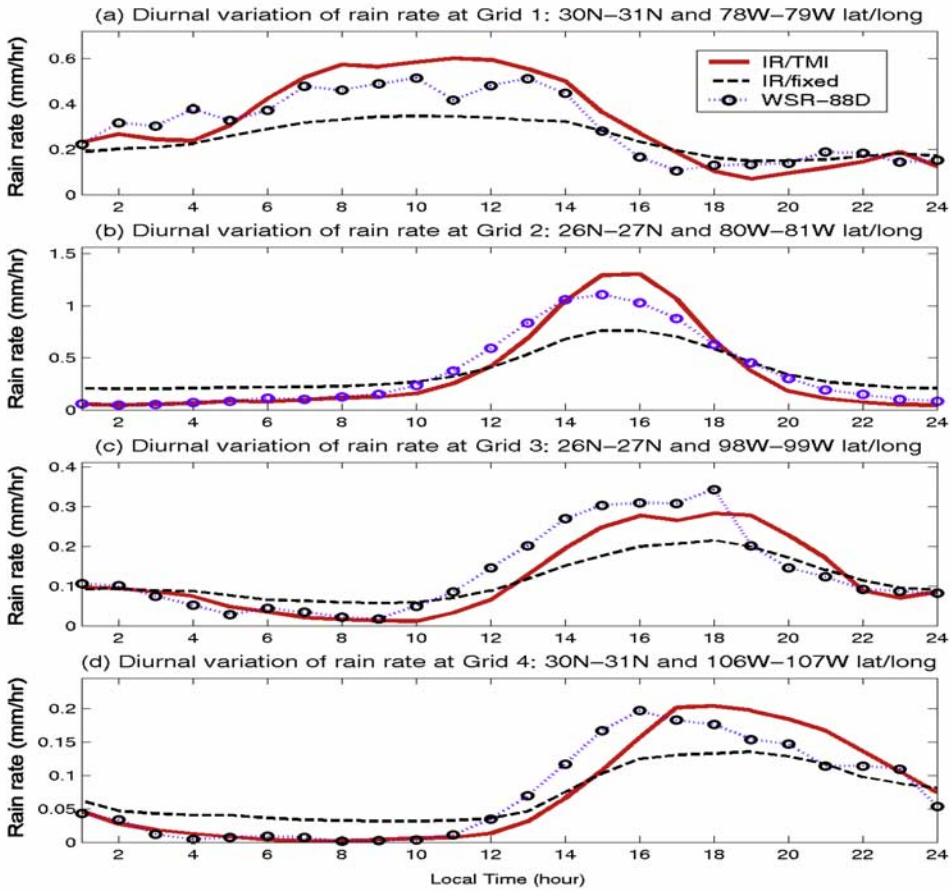

Figure 6. Comparison of diurnal variation of rainfall derived from WSR-88D radar, IR/TMI, and IR/fixed PERSIANN system over the summer season (JJA) (a–d) at four selected locations shown in Figure 2.

Table 4. Statistics of Diurnal Variation of Rain Rates From Selected Grids (1° × 1°)

	Maximum, mm hr^{-1}			Mean, mm hr^{-1}			SD		
Grid	IR/TMI	IR/Fixed	Radar	IR/TMI	IR/Fixed	Radar	IR/TMI	IR/Fixed	Radar
1	0.60	0.356	0.52	0.32	0.24	0.31	0.18	0.07	0.14
2	1.30	0.76	1.15	0.36	0.35	0.36	0.42	0.19	0.36
3	0.28	0.21	0.33	0.12	0.11	0.13	0.095	0.053	0.010
4	0.20	0.14	0.19	0.074	0.071	0.073	0.075	0.040	0.069
Mean	0.595	0.366	0.547	0.218	0.198	0.220	0.192	0.088	0.144

in a semiarid region, shows a smaller peak (0.20 mm hr^{-1}) and much lower rainfall variations throughout the day. Figure 6 illustrates that the IR/TMI rainfall in the four grids shows improvement in the depiction of the diurnal variability by more closely following the diurnal curves derived from WSR-88D data. Grids 1 and 4 also show that IR/TMI reduces the lag time of maximum peaks by 1 to 2 hours.

[25] Table 4 lists the mean of the hourly rain rates of the four grids for the IR/TMI (0.218 mm hr^{-1}). It shows lower bias than the IR/fixed rainfall (0.198 mm hr^{-1}) compared to radar data (0.220 mm hr^{-1}). The means of the maximum rain rates of the four grids are 0.595, 0.366, and 0.547 mm hr^{-1} for the IR/TMI, IR/fixed, and radar, respectively. The amplitude of the diurnal cycle from the IR/fixed rainfall is considerably less than that of the IR/TMI rainfall, varying by a ratio of 1.625:1.

4.1.3. Diurnal Variation of Rainfall From Grids Without Ground Observations

[26] For regions without reliable observation of hourly rainfall, it is expected that the IR/TMI PERSIANN will capture the diurnal variation of rainfall better than the IR/fixed PERSIANN. Two grids, A (16°N–17°N, 91°W–92°W) and B (16°N–17°N and 99°W–100°W), were selected (see Figure 2) for this purpose. Similar to the grid of Figure 6b in Florida, grid A (Figure 7a) exhibits a land pattern diurnal cycle with larger amplitude from the IR/TMI than from the IR/fixed data. Figure 7b shows grid B is an ocean pattern similar to the grid of Figure 6a for the Atlantic coast. As for the diurnal rainfall pattern over land, the IR/TMI data in grid A exhibit strong daytime convective rainfall that begins around local noon time and extends through late night with 14% of the rain falling at peak time LST 1700. However, the IR/fixed estimates follow the same shape of diurnal curve but only with 9% of rain falling at the same peak time. As for the diurnal rainfall pattern of grid B over the ocean, both estimates show weaker amplitude of maximum rainfall but longer duration of peak time, starting in the early morning through local noontime. For grid B, 9% of the total rainfall concentrates at a peak hour from the IR/TMI data, while only 6% falls at a peak time from the IR/fixed data. The IR/TMI rainfall demonstrates stronger diurnal variability of rainfall with higher maximum and lower minimum in both grids. Quantitatively, the IR/TMI data demonstrate 3–5 percentage stronger amplitude of

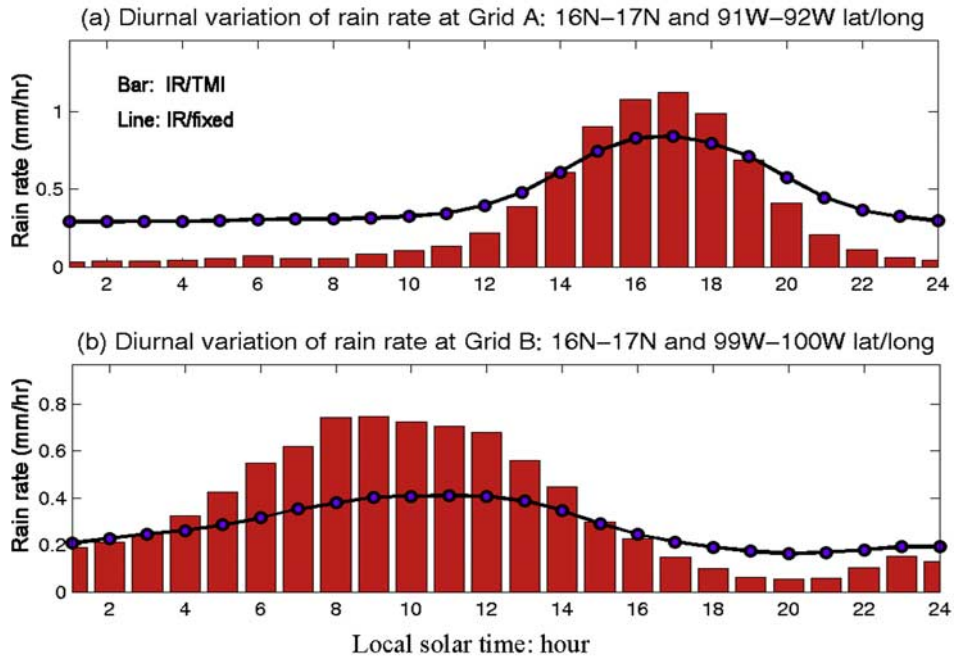

Figure 7. Diurnal variation of rainfall from with/without TMI adjustment over the summer season (JJA) at grid A (a) land and grid B (b) ocean.

peak rainfall than the IR/fixed data after normalization in these two grids.

4.2. Seasonal Signals of Diurnal Variability of Tropical Rainfall

[27] In comparison against WSR-88D observations, the incorporation of TMI-derived instantaneous rainfall measurements into the PERSIANN system improves the estimation of the key attributes of diurnal variability of rainfall, namely the amplitude and the duration of maximum rainfall.

[28] In this section, IR/TMI PERSIANN global rainfall (35°S–35°N) for the year 2002 has been processed into $1° \times 1°$ and 3-hour resolutions at local solar time for retrieval of the diurnal cycle over the boreal summer months of June, July, and August (JJA) and the winter months of December, January, and February (DJF), respectively.

[29] As shown in Figure 8a, boreal summer (JJA/austral winter) average of 3-hour rain rates indicates pronounced diurnal variability over western Mexico, Central America, the eastern Pacific Ocean, Southeast Asia, and midwestern Africa. All of these regions are characterized by marked minimum in the midmorning, maximum in the afternoon over land, and early morning maximum over the oceans. During the DJF season (austral summer) of the Southern Hemisphere (Figure 8b), Brazil and northern South America exhibit strong daytime maximum of diurnal rainfall over land, slowly decreasing through the late night. This result agrees with the finding of *Anagnostou et al.* [1999] and *Negri et al.* [2002] with respect to location and orientation of the major features. Northern Australia exhibits peak of diurnal rainfall occurring during midafternoon (1500–1800 LST) over land and early morning convection developing between 0300 and 0600 offshore. In general, land areas have higher amplitude of the diurnal cycle than the ocean due to the stronger and more frequently convective processes mostly attributed by afternoon heating over the land surface. These seasonally averaged signals of rainfall diurnal variability are in agreement, in a broad term, with previous works [*Meisner and Arkin*, 1987; *Janowiak et al.*, 1994; *Dai*, 2001; *Sorooshian et al.*, 2002; *Nesbitt and Zipser*, 2003].

5. Summary and Discussion

[30] Currently, many research teams are working on improving the accuracy and the spatial and temporal resolutions of satellite rainfall estimates for meteorological and hydrological applications. The PERSIANN system has been continuously improved in this direction [*Hsu et al.*, 1997, 1999; *Sorooshian et al.*, 2000]. The evaluation of the PERSIANN rainfall products reported here, as well as a previous publication [*Sorooshian et al.*, 2002], indicates that substantial progress has been made in the combination of multiple rainfall data sources achieved through the function of adaptability of PERSIANN network.

[31] In this study, two running modes of PERSIANN, namely simulation and update, are examined. In the simulation mode, the system transforms IR cloud-image information to rainfall through the fixed model parameters, dubbed IR/fixed PERSIANN. In the update mode, the parameters are routinely adjusted by using the coincident TMI instantaneous rain rates, namely IR/TMI PERSIANN. Consequently, two sets of 1 year (January to December 2002) of rainfall data at half-hourly $0.25° \times 0.25°$ resolution are generated from the two modes. Validation of these two data sets in comparison with rain gauge and radar observation shows that: (1) the IR/fixed PERSIANN estimation has a tendency to underestimate heavy rainfall, while the IR/TMI estimation provides better estimates for high rainfall; however, the improvement for low rainfall is marginal; (2) compared to rain gauge and radar data, the IR/TMI estimate has higher correlation (0.62 versus 0.51) and lower bias ratio (+22% versus −30%) than the IR/fixed estimate at daily $0.25° \times 0.25°$ scale; it consistently demonstrates higher correlation (0.75 versus 0.63) and lower bias ratio (+8% versus −11%) at monthly $0.25° \times 0.25°$ resolution; and (3) compared to U.S. gauge information, results show that the biased TMI retrieval technique [*Negri et al.*, 2002] introduces positive bias (22%) into the IR/TMI estimates, in contrast to the negative bias (−30%) of IR/fixed estimates.

[32] This analysis focuses on the evaluation of the quality of rainfall diurnal variability derived from the two different data products. The diurnal analysis of global tropical rainfall illustrates that the IR/TMI rainfall estimation better captures the characteristics of diurnal variability of rainfall than the IR/fixed estimation. Specific conclusions are as follows:

[33] 1. There is a strong tendency for IR/fixed data to underestimate the magnitude of rainfall diurnal variation, particularly for the peak of the diurnal cycle. However, the IR/TMI estimates show the ability to correct the tendency by 14.9% over land and 26% over coastal areas. This indicates that the routine adjustment from TMI rainfall measurements facilitates the PERSIANN to better retrieve the diurnal feature of precipitation.

[34] 2. Generally, there is a 1–3 hour lag of peak of the diurnal cycle for the two data sets (Figure 5a). Figures 6d and 7b illustrate that the IR/TMI estimates also improve phase of the diurnal cycle by reducing the lag time of peak from 2–3 hours in the IR/fixed diurnal cycles to 1–2 hours.

[35] This investigation shows the limitation of satellite IR/fixed rainfall estimation. In general, nonlinear relationships exist between cloud IR data and surface rain rates. The assumption in IR/fixed algorithms, that the colder the cloud-top temperature, the higher the surface rain rate, is not always true [*Arkin and Meisner*, 1987; *Adler et al.*, 1994]. More importantly, the IR data in fact represent the diurnal variation of cloudiness; thus the IR-only information retrieval algorithm has limited capability of overcoming the contamination by very cold anvil cirrus and the difficulty in detecting warm cloud rainfall, which particularly affects the phase of the rainfall diurnal cycle. For example, convective clouds exhibit a stronger tendency to give rise to heavy rainfall during the developing stage than during dissipating periods; this can often lead to an erroneous assignment of precipitation to cold nonprecipitating clouds or the missing of significant rainfall from tropical or subtropical warm clouds. The time lag of the peak rainfall in the diurnal cycle indicates that the peak of convective rainfall may occur before the convection reaches the highest level, suggesting that further investigation of precipitation generation in different periods of cloud life cycles would help resolve this limitation.

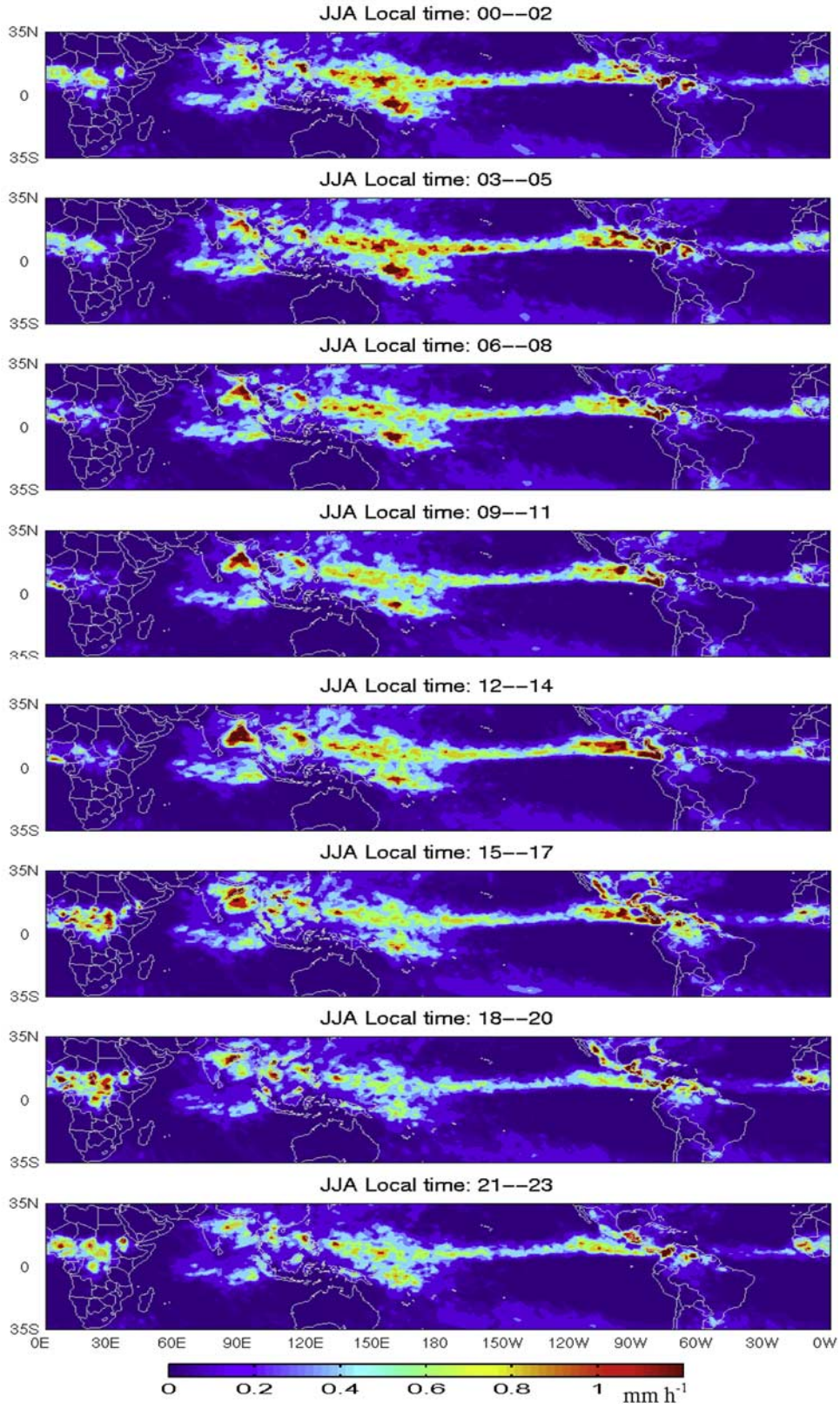

Figure 8a. Diurnal variation of global tropical rainfall from IR/TMI PERSIANN over the summer season (JJA).

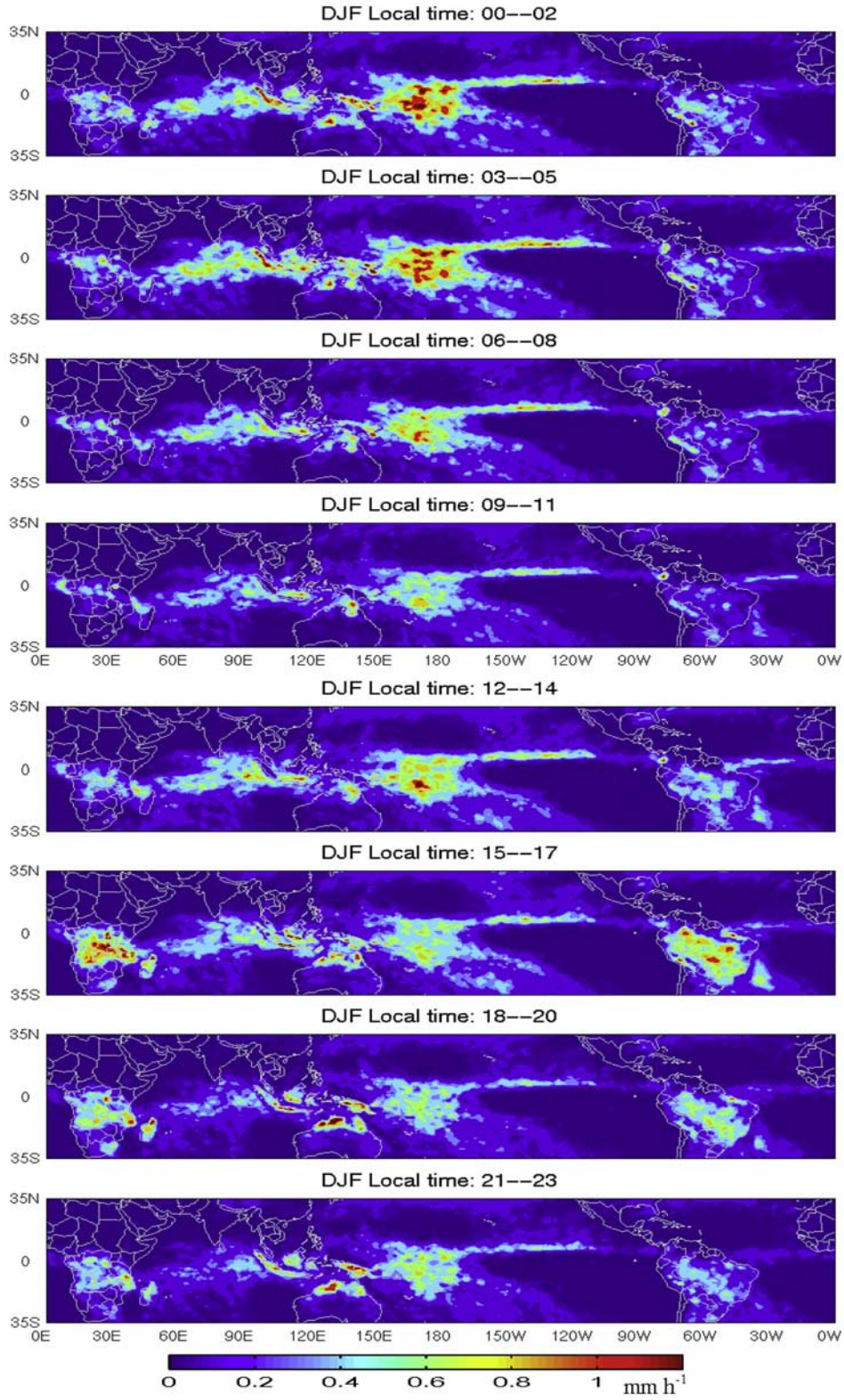

Figure 8b. Diurnal variation of global tropical rainfall from IR/TMI PERSIANN over the winter season (DJF).

[36] Further improvements may also be achieved by using more microwave rainfall data for PERSIANN parameter adjustment. With the possibility of global passive microwave composite images from TMI, Defense Meteorological Satellite Program Special Sensor Microwave Imager (SSM/I), NOAA Advanced Microwave Sounding Unit (AMSU-B), and NASA EOS Aqua Advanced Microwave Scanning Radiometer (AMSR-E),

the potential improvements in precipitation estimation accuracy and in retrieval of the diurnal cycle by using this global composite images to adjust PERSIANN network parameters is also under investigation. At the time of this writing, the last 3-year global rainfall products (at elemental 0.25° × 0.25° and 30-min resolution) from the PERSIANN algorithm, adjusted by TMI, SSM/I, and AMSU-B rainfall observations, have been processed and will be analyzed.

Appendix A: PERSIANN Network Training and Recursive Update

A1. Training of the PERSIANN Network

[37] As with any other three-layer ANN network, PERSIANN consists of an input vector $\mathbf{x} = [x_1, x_2, \ldots, x_{n0}]$ with n_0 unit neural units, an SOFM hidden layer $\mathbf{y} = [y_1, y_2, \ldots, y_{n1}]$ with n_1 node numbers, and the network output $\mathbf{z} = [z_1, z_2, \ldots, z_{n1}]$, i.e., rain rate. Defining weights w_{ji} denotes the weight connecting from the input node x_i to the SOFM node y_j and weight v_{ji} associates input x_i and output data z_{ji} through the SOFM node j.

[38] The weights **w** and **v** must be trained to group input variables **x** into one cluster of **y**; they then produce estimates of rainfall **z**. The training of the PERSIANN network proceeds through two stages: unsupervised SOFM training and a supervised linear optimization procedure.

A1.1. Unsupervised SOFM Training

[39] The procedure for training the SOFM weights vectors $\boldsymbol{w}$ is conducted as follows.

A1.1.1. Step 1

[40] Randomly initialize the $\boldsymbol{w}$ between values 0 and 1.

A1.1.2. Step 2

[41] For each input vector x_i, the "distance" between the normalized input vector and each hidden layer (SOFM) node is calculated as follows:

$$d_j = \left[\sum_{i=1}^{n0} (x_i - w_{ji})^2\right]^{0.5} \qquad j = 1, \ldots, n_1 \tag{A1}$$

A1.1.3. Step 3

[42] Select the winner node I_c such that

$$d_c = \min(d_j), \qquad j = 1, \ldots, n_1. \tag{A2}$$

A1.1.4. Step 4

[43] Update the connection weights of all hidden nodes in the neighborhood of the winning node according to the iterative adjustment rule (the nodes outside $\Omega_c(m)$ remain the same as before):

$$w_{ji}(m) = w_{ji}(m-1) + \eta(m)\left[x_i - w_{ji}(m-1)\right], \text{if } j \in \Omega_c(m); \quad \text{otherwise } w_{ji}(m) = w_{ji}(m) \tag{A3}$$

where m is the training iteration index, $\eta(m)$ is the learning rate, and $\Omega_c(m)$ defines the neighborhood size around the winning node I_c. The initial settings of the learning rate η_0 is 0.2–0.5 and the neighborhood size Ω_c is $n_1/2$, i.e., half of the SOFM node size. As the training proceeds, both the $\Omega_c(m)$ and $\eta(m)$ progressively decrease until the values of the weights $\boldsymbol{w}$ stabilize.

A1.2. Supervised Linear Optimization Procedure in the Output Layer

[44] After the SOFM training, the linear equation (A4) associates input and output data at node j, and the weights v_{ji} can be determined using a straightforward "supervised learning" strategy given concurrently collocated rainfall observations.

$$z = \sum_{i=1}^{n0} v_{ji} x_i \quad if \quad j = c; \quad \text{otherwise}, \quad z = 0 \tag{A4}$$

A2. Adaptation of the PERSIANN System (Update Mode)

[45] The procedure of training the weights w_{ji} and v_{ji} is quite straightforward and is discussed above. Note that, while the SOFM weights w_{ji} must be trained off line, the weights v_{ji} can be first initialized through off-line training and then recursively updated by a sequential online training procedure that makes small adjustments to the parameters in the neighborhood of an active node through an error feedback process using the Widrow-Hoff learning rule. The weight update is taken from the negative gradient direction of matching error associated with the update weight, v_{ji}, as shown in equation (A5).

$$v_{ji}^{new} = v_{ji}^{old} + \eta[t_{obs} - z_{sim}]y_j \quad if\ j = \Omega; \quad otherwise, \quad v_{ji}^{new} = v_{ji}^{old} \tag{A5}$$

where t_{obs} is observed rainfall such as microwave or ground-truth data, z_{sim} is the simulated PERSIANN rainfall estimates without adjustment, and η is the learning rate between 0 and 1. The value of y_j is dependent on the competition of the SOFM layer. A value of 1.0 is assigned to the winner node, I_c, which has minimum distance between inputs, **x**, and the SOFM connection weight, **w**. The value of y_j is 0.0 in all nodes other than the neighborhood of the winner node. As a result, only the weights at $j = I_c$ and within its neighborhood Ω are adjusted; other weights remain at the previous values.

[46] As a result, the simulation mode of PERSIANN generates rainfall estimates with the fixed network parameters using an off-line training procedure, while the update mode produces rainfall with the adjusted parameters through an online recursive updating procedure. This process of recursive updating enables the estimates of PERSIANN rainfall to track and adjust to temporal and spatial variation in the rainfall distribution.

[47] **Acknowledgments.** The authors wish to acknowledge Phillip A. Arkin and the other peer reviewers for their constructive and helpful comments and suggestions. Partial support for this research is from NASA-EOS grant (NA56GPO185) and NASA TRMM project (NAG5-7716).

References

Adler, R. F., G. F. Huffman, and P. R. Keehn (1994), Global tropical rain estimates from microwave-adjusted geosynchronous data, *Remote Sens. Rev.*, *11*, 125–152.

Anagnostou, E. N., A. Negri, and R. Adler (1999), Satellite observations of the diurnal variability of rainfall in Amazonia, *J. Geophys. Res.*, *104*(D24), 31,477–31,488.

Arkin, P. A., and B. N. Meisner (1987), The relationship between large-scale convective rainfall and cold cloud over the Western Hemisphere during 1982–84, *Mon. Weather Rev.*, *115*(1), 51–74.

Bellerby, T. J., M. Todd, D. Kniveton, and C. Kidd (2000), Rainfall estimation from a combination of TRMM precipitation radar and GOES multispectral satellite imagery through the use of an artificial neural network, *J. Appl. Meteorol.*, *39*, 2115–2128.

Dai, A. (2001), Global precipitation and thunderstorm frequencies, part II: Diurnal variations, *J. Clim.*, *14*, 1112–1128.

Ebert, E. E. (1996), Results of the 3rd Algorithm Intercomparison Project (AIP-3) of the Global Precipitation Climatology Project (GPCP), *Rep. 55*, 204 pp., Bur. of Meteorol. Cent., Melbourne, Victoria.

Ebert, E. E., and M. J. Manton (1998), Performance of satellite rainfall estimation algorithms during TOGA COARE, *J. Atmos. Sci.*, *55*, 1537–1557.

Hong, Y., K. L. Hsu, and S. Sorooshian (2003), A combined microwave and IR rainfall estimation algorithm using a cloud classification system, paper presented at 30th International Symposium on Remote Sensing of Environment, Int. Cent. for Remote Sens. of the Environ., Honolulu, Hawaii, 10–14 Nov.

Hong, Y., K. L. Hsu, S. Sorooshian, and X. Gao (2004), Precipitation estimation from remotely sensed information using artificial neural network cloud classification system, *J. Appl. Meteorol.*, *43*(12), 1834–1853.

Hsu, K., X. Gao, S. Sorooshian, and H. V. Gupta (1997), Precipitation estimation from remotely sensed information using artificial neural networks, *J. Appl. Meteorol.*, *36*, 1176–1190.

Hsu, K., H. V. Gupta, X. Gao, and S. Sorooshian (1999), Estimation of physical variables from multichannel remotely sensed imagery using a neural network: Application to rainfall estimation, *Water Resour. Res.*, *35*(5), 1605–1618.

Hsu, K., H. V. Gupta, X. Gao, S. Sorooshian, and B. Imam (2002), Self-organizing linear output (SOLO): An artificial neural network suitable for hydrologic modeling and analysis, *Water Resour. Res.*, *38*(12), 1302, doi:10.1029/2001WR000795.

Huffman, G. J., R. F. Adler, B. Rudolf, U. Schneider, and P. R. Keehn (1995), Global precipitation estimates based on a technique for combining satellite-based estimate, rain gauge analysis, and NWP model precipitation information, *J. Clim.*, *8*, 1284–1295.

Huffman, G. J., R. Adler, M. Morrissey, D. Bolvin, S. Curtis, R. Joyce, B. McGavock, and J. Susskind (2001), Global precipitation at one-degree daily resolution from multisatellite observations, *J. Hydrometeorol.*, *2*, 36–50.

Janowiak, J. E., P. A. Arkin, and M. Morrissey (1994), An examination of the diurnal cycle in oceanic tropical rainfall using satellite and in situ data, *Mon. Weather Rev.*, *122*(10), 2296–2311.

Janowiak, J. E., R. J. Joyce, and Y. Yarosh (2001), A real-time global half-hourly pixel resolution IR dataset and its applications, *Bull. Am. Meteorol. Soc.*, *82*, 205–217.

Joyce, R. J., J. E. Janowiak, P. A. Arkin, and P. Xie (2004), CMORPH: A method that produces global precipitation estimates from passive microwave and infrared data at high spatial and temporal resolution, *J. Hydrometeorol.*, *5*, 487–503.

Kidd, C., D. R. Kniveton, M. C. Todd, and T. J. Bellerby (2003), Satellite rainfall estimation using combined passive microwave and infrared algorithms, *J. Hydrometeorol.*, *4*(6), 1088–1104.

Kuligowski, R. J. (2002), A self-calibrating real-time GOES rainfall algorithm for short-term rainfall estimates, *J. Hydrometeorol.*, *3*, 112–130.

Kummerow, C., and L. Giglio (1995), A method for combining passive microwave and infrared rainfall observations, *J. Atmos. Oceanic Technol.*, *12*, 33–45.

Kummerow, C., W. Barnes, T. Kozu, J. Shiue, and J. Simpson (1998), The Tropical Rainfall Measuring Mission (TRMM) sensor package, *J. Atmos. Oceanic Technol.*, *15*, 809–817.

Kummerow, C., Y. Hong, W. S. Olson, S. Yang, R. F. Adler, J. McCollum, R. Ferraro, G. Petty, and T. T. Wilheit (2001), The evolution of the Goddard Profiling Algorithm (GPROF) for rainfall estimation from passive microwave sensors, *J. Appl. Meteorol.*, *40*, 1801–1820.

Maddox, R. A., J. Zhang, J. J. Gourley, and K. W. Howard (2002), Weather radar coverage over the contiguous United States, *Weather Forecast.*, *17*(4), 927–934.

Meisner, B. N., and P. A. Arkin (1987), Spatial and annual variations in the diurnal cycle of large-scale tropical convective cloudiness and precipitation, *Mon. Weather Rev.*, *115*(9), 2009–2032.

Miller, S. W., P. A. Arkin, and R. Joyce (2001), A combined microwave/infrared rain rate algorithm, *Int. J. Remote Sens.*, *22*(17), 3285–3307.

Negri, A. J., T. L. Bell, and L. Xu (2002), Sampling of the diurnal cycle of precipitation using TRMM, *J. Atmos. Oceanic Technol.*, *19*(9), 1333–1344.

Nesbitt, S. W., and E. J. Zipser (2003), The diurnal cycle of rainfall and convective intensity according to three years of TRMM measurements, *J. Clim.*, *16*, 1456–1475.

Sorooshian, S., K. Hsu, X. Gao, H. V. Gupta, B. Imam, and D. Braithwaite (2000), Evolution of the PERSIANN system satellite-based estimates of tropical rainfall, *Bull. Am. Meteorol. Soc.*, *81*(9), 2035–2046.

Sorooshian, S., X. Gao, K. Hsu, R. A. Maddox, Y. Hong, H. V. Gupta, and B. Imam (2002), Diurnal variability of tropical rainfall retrieved from combined GOES and TRMM satellite information, *J. Clim.*, *15*(9), 983–1001.

Xie, P., and P. A. Arkin (1996), Analyses of global monthly precipitation using gauge observations, satellite estimates, and model predictions, *J. Clim.*, *9*, 840–858.

Xu, L., X. Gao, S. Sorooshian, P. A. Arkin, and B. Imam (1999), A microwave infrared threshold technique to improve the GOES Precipitation Index, *J. Appl. Meteorol.*, *38*, 569–579.

X. Gao, Y. Hong, K.-L. Hsu, and S. Sorooshian, Center for Hydrometeorology and Remote Sensing, Department of Civil and Environmental Engineering, University of California, Irvine, CA 92697, USA. (soroosh@uci.edu)